



Extreme mechanical anisotropy in diamond with preferentially oriented nanotwin bundles

Yilong Pan^{a,1}, Pan Ying^{a,b,1}, Yufei Gao^{a,b,1}, Peng Liu^{c,1}, Ke Tong^{a,2}, Dongli Yu^a, Kaili Jiang^c, Wentao Hu^a, Baozhong Li^a, Bing Liu^a, Zhisheng Zhao^{a,2}, Julong He^a, Bo Xu^{a,2}, Zhongyuan Liu^a, and Yongjun Tian^a

^aCenter for High Pressure Science, State Key Laboratory of Metastable Materials Science and Technology, Yanshan University, Qinhuangdao, Hebei 066004, China; ^bKey Laboratory of Microstructural Material Physics of Hebei Province, School of Science, Yanshan University, Qinhuangdao 066004, China; and ^cState Key Laboratory of Low-Dimensional Quantum Physics, Department of Physics and Tsinghua-Foxconn Nanotechnology Research Center, Tsinghua University, Beijing 100084, China

Edited by Ho-kwang Mao, Center for High Pressure Science and Technology Advanced Research, Beijing, China, and approved October 19, 2021 (received for review May 3, 2021)

Mechanical properties of covalent materials can be greatly enhanced with strategy of nanostructuring. For example, the nanotwinned diamond with an isotropic microstructure of interweaved nanotwins and interlocked nanograins shows unprecedented isotropic mechanical properties. How the anisotropic microstructure would impact on the mechanical properties of diamond has not been fully investigated. Here, we report the synthesis of diamond from superaligned multiwalled carbon nanotube films under high pressure and high temperature. Structural characterization reveals preferentially oriented diamond nanotwin bundles with an average twin thickness of ca. 2.9 nm, inherited from the directional nanotubes. This diamond exhibits extreme mechanical anisotropy correlated with its microstructure (e.g., the average Knoop hardness values measured with the major axis of the indenter perpendicular and parallel to nanotwin bundles are 233 ± 8 and 129 ± 9 GPa, respectively). Molecular dynamics simulation reveals that, in the direction perpendicular to the nanotwin bundles, the dense twin boundaries significantly hinder the motion of dislocations under indentation, while such a resistance is much weaker in the direction along the nanotwin bundles. Current work verifies the hardening effect in diamond via nanostructuring. In addition, the mechanical properties can be further tuned (anisotropy) with microstructure design and modification.

diamond | preferential orientation | nanotwin bundles | mechanical properties | anisotropy

The combination of exceptional properties, such as the highest hardness, incompressibility and thermal conductivity, large band gap and electric breakdown field, and wide optical transparency, make diamond a unique material for a diversity of applications, including cutting tools and wear protection, thermal management, optical components, and semiconductor devices, etc. Therefore, synthesizing diamond materials with an enhanced comprehensive performance superior to monocrystalline diamond has been a long-lasting goal since the first synthesis of man-made diamond (1). Previous progress has indicated that the mechanical performance of covalent materials can be greatly enhanced with strategy of nanostructuring (2–6). For example, the synthetic nanopolycrystalline diamond (NPD) and nanotwinned diamond (nt-diamond) exhibit superb mechanical properties (2, 5), with an unprecedented hardness of 200 GPa (twice that of natural diamond single crystal) achieved in nt-diamond. In both nt-diamond and NPD, randomly oriented equiaxed grains (with or without subgrained nanotwins) integrate into a bulk with an isotropic microstructure, leading to isotropic mechanical properties in contrast to the anisotropy in diamond single crystals.

Along with the enhancement of properties, the fine tuning of material performance with microstructure design and regulation has become increasingly important. For example, materials with an anisotropic structure or a hierarchical integrated

structure play an important role in certain sites, such as anisotropic filtering (7), etching techniques (8), and biological systems (9), in which ordinary isotropic materials usually cannot provide. Studies of hardness anisotropy have been conducted mainly on single crystals [e.g., minerals (10–13)]. It is well known that anisotropy in metallic materials can be achieved by processing techniques, such as hot rolling, wire drawing, and heat treatments (14). These techniques, however, cannot be applied to hard and brittle ceramic materials, such as diamond and cubic boron nitride. Previously, a nanolayered diamond compact was synthesized by direct conversion from highly oriented pyrolytic graphite (15), exhibiting an anisotropic microstructure of layered crystals (50 to 100 nm thick) and a mild anisotropy in hardness measured on the top surface (114 GPa) and side face (95 GPa). This limited hardness anisotropy can be ascribed to the relatively large grain size, contributing to a slight variation in hardness. Nonetheless, these previous works inspired us the possibility to modulate the diamond microstructure by choosing appropriate precursors (2, 5, 15–18). Considering the hardening effect of the twin boundary (TB) similar to that of grain boundary (19) and the intrinsic anisotropic nature of TB, enhanced mechanical properties as well as extreme

Significance

Diamond is an essential material for industrial and scientific applications due to its exceptional properties. The regulation of diamond performance through microstructural design is a challenging and hot topic. Here, we report the synthesis of diamond with preferentially oriented nanotwin bundles via direct phase transformation of superaligned multiwalled carbon nanotube films under high temperature and pressure. The preferentially oriented nanotwin bundles endow diamond with the highest hardness anisotropy ever recorded and a record hardness value in the direction perpendicular to the oriented nanotwin bundles. Current findings provide valuable insights on the microstructural design and modification of diamond and related materials, contributing to the further tuning of properties in the future.

Author contributions: P.L., K.J., Z.Z., B.X., and Y.T. designed research; Y.P., P.Y., P.L., B. Li, and B. Liu performed research; K.T. and W.H. contributed new reagents/analytic tools; Y.P., P.Y., K.T., D.Y., W.H., Z.Z., J.H., B.X., and Z.L. analyzed data; and Y.P., P.Y., Y.G., Z.Z., and B.X. wrote the paper.

The authors declare no competing interest.

This article is a PNAS Direct Submission.

Published under the PNAS license.

¹Y.P., P.Y., Y.G., and P.L. contributed equally to this work.

²To whom correspondence may be addressed. Email: tongke@ysu.edu.cn, zzhao@ysu.edu.cn, or bxu@ysu.edu.cn.

This article contains supporting information online at <http://www.pnas.org/lookup/suppl/doi:10.1073/pnas.2108340118/-DCSupplemental>.

Published November 15, 2021.

mechanical anisotropy can potentially be achieved via construction of a microstructure with highly oriented nanotwins.

Here, we demonstrate the successful synthesis of diamond with preferentially oriented nanotwinned microstructures from superaligned multiwalled carbon nanotube (MWCNT) films through phase transformation under high pressure and high temperature (HPHT). Transmission electron microscopy (TEM) characterization reveals a unique microstructure of the synthetic diamond (i.e., the preferentially oriented nanotwin bundles are closely related to the precursor of superaligned MWCNT films). This diamond exhibits extreme mechanical anisotropy with respect to the orientation of nanotwin bundles. Notably, the maximum Knoop hardness reaches as high as 241 GPa, with the long diagonal of the indenter perpendicular to the nanotwin bundles, more than 20% higher than the previous record (5), benefited from the very small twin thickness of 2.9 nm. The molecular dynamics (MD) simulation of the indentation process also confirms the variation trend of hardness with respect to the nanotwin bundles. Moreover, TEM observations of the cracks induced by the indentation fracture toughness measurements indicate that crack propagation is severely constrained in the direction perpendicular to the nanotwin bundles, while much less constrained in the direction along the TBs because of the different resistance of the TBs. As a result, the

crack length in the former direction is much shorter than that in the latter one.

Results and Discussion

Previous studies have demonstrated that diamond products with completely different microstructures can be produced from distinct carbon precursors such as graphite and onion-like carbon (2, 5). Graphite-like precursors tend to transform into nanograined diamond (2), while carbon onions as precursor produced nanotwins within the interlocked nanograins of diamond (5). Single-walled CNTs (SWCNTs) and MWCNTs have also been actively studied under HPHT conditions in the past few decades (20–23). For example, MWCNTs can completely transform into a sp^3 -hybridized carbon phase under nonhydrostatic pressure up to 16 GPa (23). In this work, superaligned MWCNT precursors were subjected to HPHT. MWCNTs with a transverse cross section similar to that of carbon onions can extend a long distance in the axial direction, indicating the potential to form nanotwin domains with larger width or length. MWCNT films (Fig. 1A) were drawn from superaligned MWCNT arrays (24), folded into disks 2 mm in diameter, and used as the precursor for HPHT experiments. A typical nanotube (9 walls with an inner diameter of 5.6 nm and outer diameter of 11.4 nm) is shown in Fig. 1A, *Inset*. Compared with the

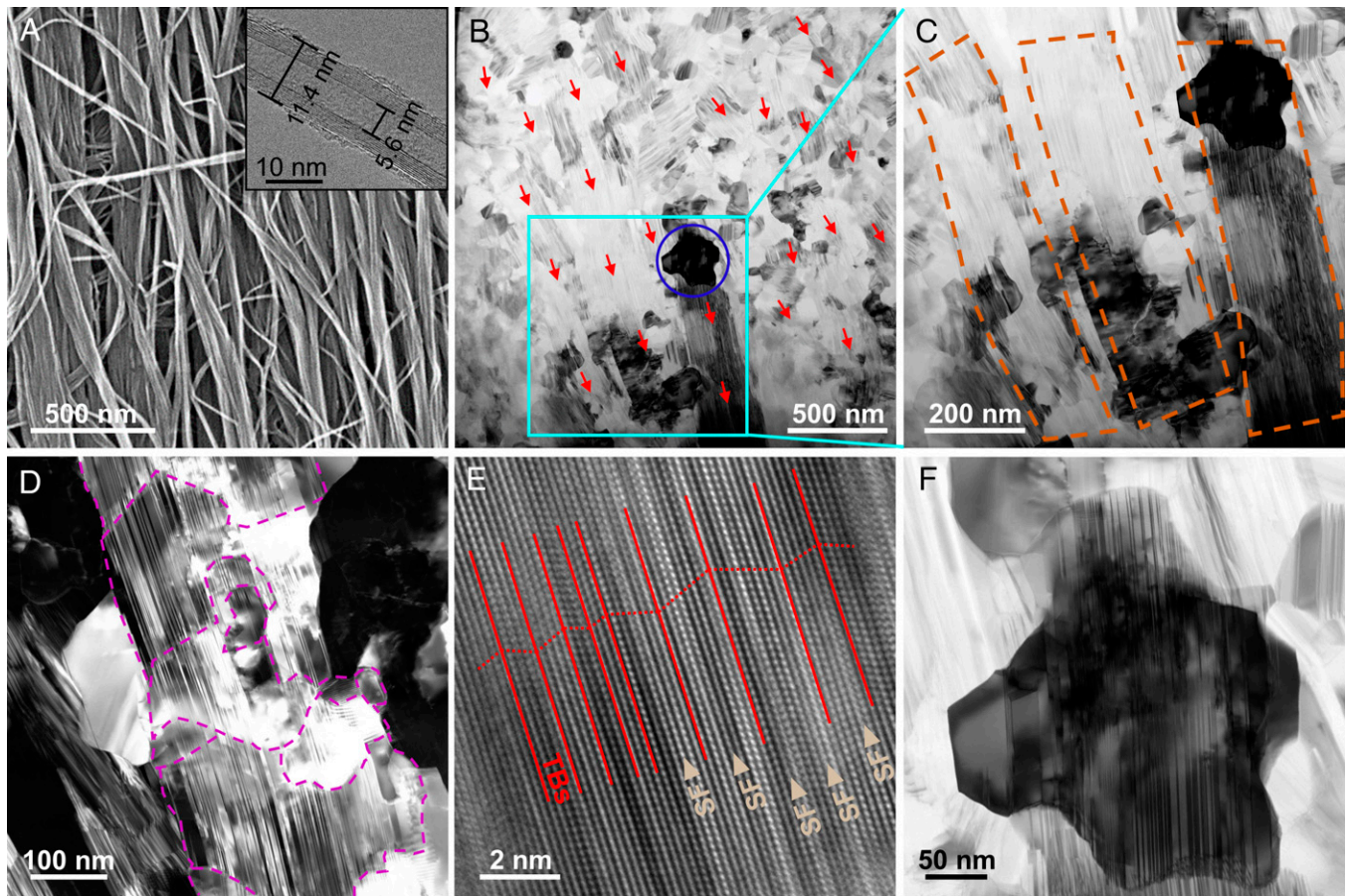


Fig. 1. Microstructures of superaligned MWCNT films and a bulk sample synthesized at 15 GPa and 2,100 °C. (A) SEM image of MWCNT films. The inset shows an HRTEM image of a single MWCNT with inner and outer diameters of 5.6 and 11.4 nm, respectively. (B) BF-STEM image of the synthetic diamond showing a bundle-like microstructure. The red arrows signify the orientations of the striped features. (C) BF-STEM image from the cyan-boxed region in B, clearly revealing micrometer-sized preferentially oriented nanotwin bundles running across multiple diamond nanograins. The twins in each bundle (cf. dashed polygons) are coherently related, implying they may come from the same MWCNT film in the precursor. (D) Annular dark field STEM (ADF-STEM) image of a region where striped and coherently interfaced nanotwins penetrate several diamond nanograins. The grain boundaries are marked with purple dashed lines. (E) HRTEM image of the nanotwin bundles. TBs (red solid lines) and stacking faults (SFs; arrowheads) are marked. (F) BF-STEM image of a typical nanograin (the blue circle in B). The preferentially oriented nanotwins traveling through the nanograin can be clearly observed.

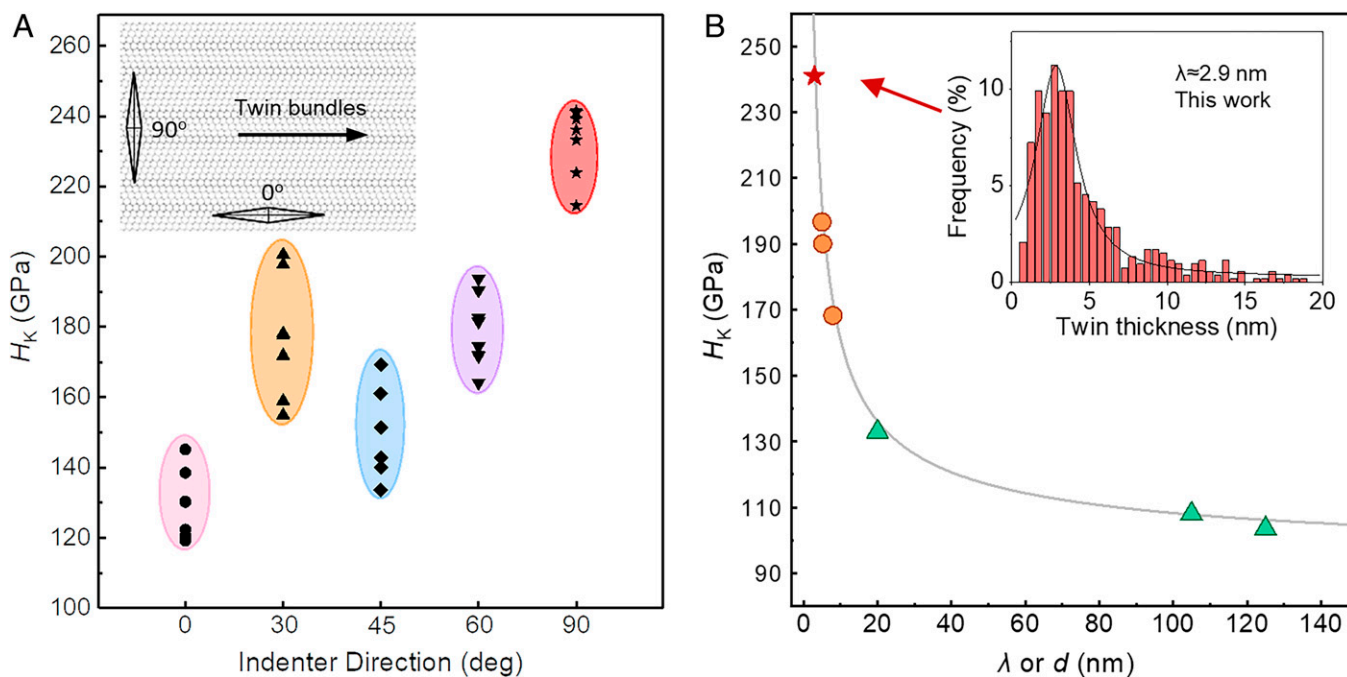


Fig. 2. Knoop hardness of the diamond with a preferentially oriented twinning microstructure. (A) Knoop hardness as a function of the misaligned angle between the major diagonal of the Knoop indenter and $\{111\}$ TBs of the nanotwin bundles (see the *Inset* for the definition), revealing a significant hardness anisotropy. (B) Hardness as a function of average grain size (d) or twin thickness (λ) for nanostructured diamond bulk materials. The circles and triangles are experimental data from nt-diamond (5) and nanograined diamond (2), respectively. The *Inset* shows the twin thickness distribution in the diamond with preferentially oriented nanotwin bundles from HRTEM observations. The average twin thickness is about 2.9 nm, accounting for the ultra-high Knoop hardness of 241 GPa measured along the direction perpendicular to the nanotwin bundles.

carbon onions with a size of 20 to 50 nm used to produce nt-diamond (5), the MWCNTs used in this work possess similar concentric carbon shells but a much higher curvature, implying an easy transformation into twin substructures.

X-ray diffraction patterns of the MWCNT precursor and the sample recovered from the 15 GPa and 2,100 °C treatment are displayed in *SI Appendix, Fig. S1*. The recovered sample shows a pure cubic diamond phase, indicating a complete transformation from MWCNT to diamond. TEM observations (Fig. 1 B–F) reveal plentiful striped features that characterize the microstructure of this diamond. These stripes are preferentially oriented with lengths of up to 1 μm and penetrate diamond nanograins frequently (Fig. 1 B–D). The high-resolution TEM (HRTEM) image shown in Fig. 1E discloses that the stripes are assembled from a bundle of diamond nanotwins with many stacking faults. The thickness distribution, based on HRTEM observation of more than 500 nanotwins, indicates an average twin thickness of 2.9 nm (Fig. 2B, *Inset*). Moreover, the bright-field scanning TEM (BF-STEM) image shows the details of a nanograin penetrated by the nanotwin bundle (Fig. 1F). It is clear that nanotwins within the nanograin also show a preferential orientation, in sharp contrast to the randomly oriented nanotwins in diamonds transformed from carbon onions (5). The diamond sample produced from these MWCNTs, therefore, possesses a unique anisotropic microstructure featured with preferentially oriented nanotwin bundles, differing from the isotropic microstructure in previously reported nt-diamond (5).

From the positioning label on the BN crucible (*Sample Preparation*), we can determine the orientation of diamond nanotwin bundles is consistent with that of MWCNT films. The specific orientations of the nanotwin bundles vary slightly in different diamond domains. Nonetheless, individual domains composed of nanotwins with identical orientation usually span 2 to 10 μm longitudinally and ca. 200 nm crosswise (Fig. 1C), which

is directly related to the dimensions of the MWCNT films (Fig. 1A). These consistencies provide a useful clue for understanding the mechanism of the transformation of MWCNT films to diamond with preferentially oriented nanotwins. In the precursor films, individual MWCNTs with diameters of 7 to 12 nm were assembled into parallel-aligned films. Under HPHT conditions, the tabular MWCNTs constituting of multiple, nested SWCNTs underwent radical deformation and collapsed in a similar manner to carbon onions due to their structural similarity, forming nanotwins with preferentially TBs oriented along the tube direction. A schematic diagram of the transformation process from a single (17,0)/(26,0)/(35,0) triple-walled CNT to diamond nanotwins under uniaxial compression is presented in *SI Appendix, Fig. S2*.

To investigate the mechanical properties of current diamond samples as well as the correlation with the unique anisotropic microstructure, Knoop hardness measurements were performed on the polished surface with the determined preferential nanotwins orientation. Note the Knoop indenter has an elongated rhombic base with a length to width ratio of 7:1, which helps to detect possible hardness anisotropy in tested samples (13, 25). The indentation hardness (Vickers or Knoop) can be measured reliably as long as a permanent plastic impression can be formed on the surface of the tested sample with no visible plastic deformation of diamond indenter (26). The principle of indentation hardness measurement and Knoop indenter characterization before and after the hardness measurement can be found in *SI Appendix, Fig. S7*. A misaligned angle between the long diagonal of Knoop indenter and the oriented nanotwins was defined before hardness measurement (i.e., 0° for the parallel case and 90° for the perpendicular one). The misaligned, angle-dependent Knoop hardness is shown in Fig. 2A, disclosing a remarkable anisotropy in Knoop hardness. Generally speaking, the hardness value increases with a larger misaligned angle: The extreme hardness values are 129 ± 9 and

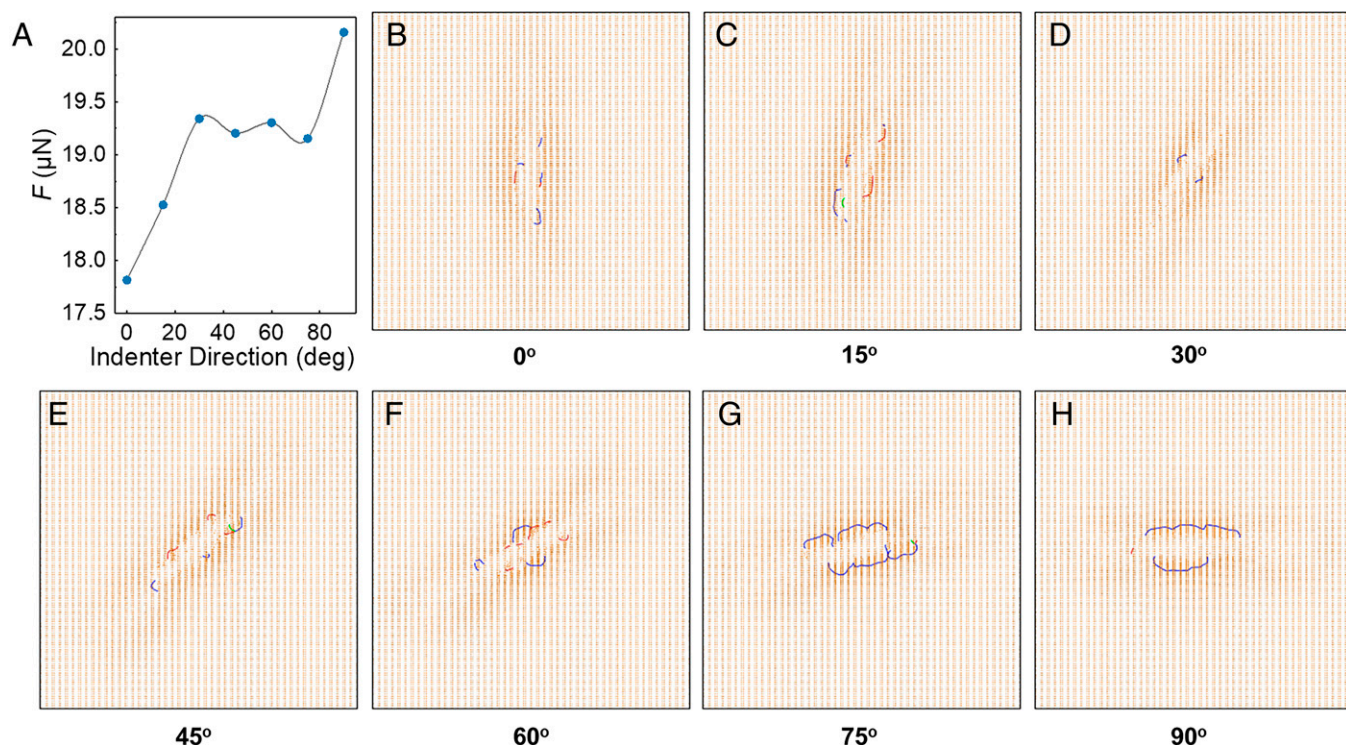


Fig. 3. MD simulation of hardness tests on diamond with a preferentially oriented twinning microstructure. (A) Loading force as a function of misaligned angle between the major diagonal of the indenter and $\{111\}$ TBs of the nanotwin bundles. Note that an identical indentation depth was used for the simulation, and the calculated force is therefore directly proportional to the hardness. The variation of hardness with the misaligned angle is consistent with the experimental results. (B–H) Dislocation distribution in the vicinity of the indentation with identical indentation depth. The misaligned angle increases from 0° (B) to 90° (H). At 0° , dislocations are mainly distributed along twin boundaries, while at 90° , the dislocations traverse several TBs and curve after intersecting TBs, indicating TBs can significantly hinder the motion of dislocation and contribute to hardening. The orange atoms and blue lines represent twin boundaries and dislocations, respectively.

233 ± 8 GPa corresponding to 0° and 90° , respectively. The anisotropy in hardness exhibited in current diamond with a preferentially oriented nanotwinned microstructure was absent in the previously reported nt-diamond with randomly oriented nanotwins synthesized from carbon onions (5). *SI Appendix, Fig. S3* displays a series of indentations from Knoop hardness measurements with different misaligned angles.

Previously, we proposed a hardness model for polycrystalline covalent materials considering hardening contributions from the Hall–Petch effect and the quantum confinement effect (6, 27) [i.e., $H = H_0 + K_{\text{HP}}D^{-1/2} + K_{\text{qc}}D^{-1}$, where D (in nanometer) is the grain size or twin thickness], H_0 , K_{HP} , and K_{qc} are 90 GPa, 164 GPa/nm $^{1/2}$, and 189.7 GPa/nm, respectively, for nanostructured diamond (6). For the 90° Knoop hardness measurement, the resistance to plastic deformation is dominated by the TBs that hinder dislocation motion and crack propagation. A hardness value as high as 251 GPa can be estimated from the above formula assuming an average twin thickness of 2.9 nm. However, for the 0° Knoop hardness measurement, the grain boundaries play a leading role in hindering dislocation motion and crack propagation. With an average grain size of 44.3 nm (*SI Appendix, Fig. S4*), the Knoop hardness at a misaligned angle of 0° is estimated as 120 GPa. Both values are in good agreement with the experimental extremes. Notably, the maximal Knoop hardness of 241 GPa is 20% higher than the previous record achieved in nt-diamonds (5), obviously benefited from the smaller twin thickness.

To further understand the effect of oriented TBs on Knoop hardness of diamond, we simulated the measurement process of a model diamond sample composed of oriented twins with MD (see *Materials and Methods* for the details). The minimal

twin thickness of 0.618 nm (i.e., $3d_{111}$) was used in the diamond model. During the simulation, the misaligned angle varied from 0° (parallel) to 90° (perpendicular). For each misaligned angle, the indenting depth was set as 0.8 nm, and then the force acting on the indenter was calculated. From here, the variation trend of hardness with respect to the misaligned angle can be qualitatively characterized. As shown in Fig. 3A, the loading force varies as a function of the misaligned angle, revealing a trend consistent with the Knoop hardness measurements (Fig. 2A). Fig. 3 B–H highlights the dislocation behavior at different misaligned angles. We do notice some irregularity for the middle-range misaligned angles, such as hardness in 30 to 60° (Fig. 2A) and loading force in 30 to 75° (Fig. 3A). The variation in hardness of the diamond with preferentially oriented nanotwin bundles can be attributed to two main factors (i.e., the twin strengthening and the dislocation density). With larger misaligned angle, the twin strengthening play an increasingly important role, resulting in the overall increase trend of hardness. When the misaligned angle is in the range of 30 to 75° , the dislocation density increases substantially with increasing misaligned angle (Fig. 3 D–F), thus contributing a decrease in hardness. The joint contribution from twin strengthening (hardening) and the dislocation density (softening) then results in the small irregularity of loading force (or hardness) in 30 to 75° .

SI Appendix, Fig. S5 shows a micrograph of Vickers indentation after the fracture toughness measurement. The two indentation diagonals are parallel and perpendicular to the oriented nanotwin bundles. It is clear that the average length of the radial cracks measured from the indentation center significantly differ: the average length is 7.2 μm in the direction

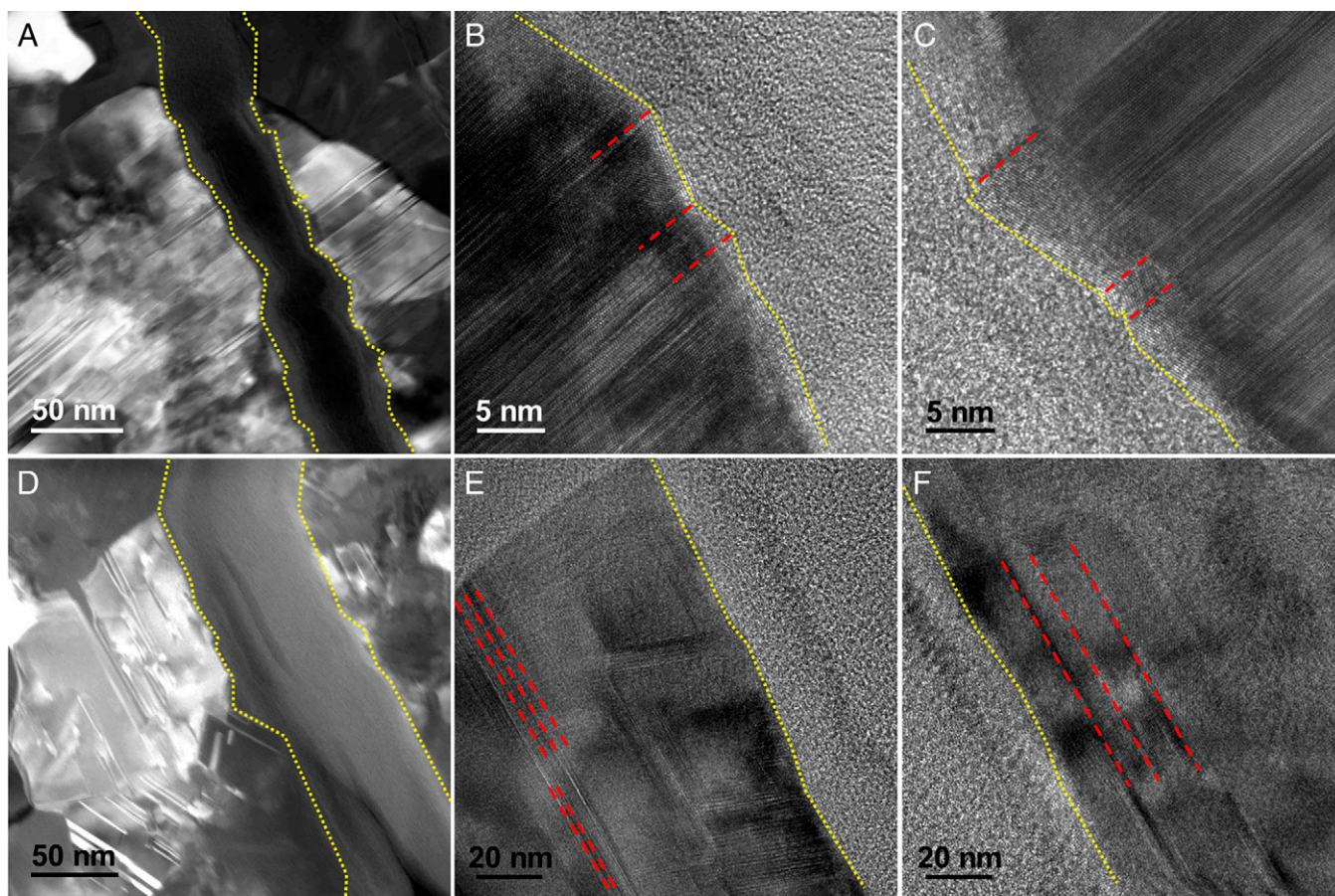


Fig. 4. Crack propagation behavior in the directions perpendicular or parallel to the nanotwin bundles. (A–C) ADF-STEM (A) and HRTEM (B and C) images of a crack propagating in the direction perpendicular to the nanotwin bundles. The continuous deflections at the twin boundaries (red dotted line) leads to a zigzag propagation path (yellow dotted line), which dissipates substantial energy and thus increases the resistance to crack propagation (toughening). (D–F) ADF-STEM (D) and HRTEM (E and F) images of a crack propagating in the direction parallel to the nanotwin bundles. The crack tends to extend along the TB, leading to straight fracture surfaces and less resistance to crack propagation.

perpendicular to the oriented nanotwin bundles and $15.8 \mu\text{m}$ in the parallel direction. In other words, crack propagation was significantly impeded in the direction perpendicular to the nanotwin bundles. TEM characterization of the indentation cracks was performed to clarify the distinct behaviors of crack propagation in the two directions (Fig. 4). In the direction perpendicular to the oriented nanotwin bundles, the crack was continuously deflected at the TBs and propagated in a zigzag path, similar to what occurred in 3-C diamond nanotwins regions observed previously (28). Such continuous crack deflections at the TBs can dissipate substantial strain energy and resist crack propagation. Contrastively, in the direction parallel to the nanotwin bundles, the crack propagated along the TBs in an almost straight line (i.e., $\{111\}$ planes of diamond), leading to much longer cracks without obvious impediment.

Conclusion

In summary, diamond with preferentially oriented nanotwin bundles were synthesized from superaligned MWCNT films. These nanotwin bundles have an average twin thickness of 2.9 nm, which is closely related to the small transverse section of MWCNTs. The mechanical properties of the diamond show extreme anisotropy correlated with the unique microstructure. The Knoop hardness reaches $233 \pm 8 \text{ GPa}$ with the long axis of the indenter perpendicular to nanotwin bundles while $129 \pm 9 \text{ GPa}$ with the long axis parallel to nanotwin bundles. Also, crack propagation exhibits significant anisotropy along the direction

perpendicular or parallel to the nanotwin bundles. MD simulation and TEM characterization attribute these anisotropic mechanical properties to the practical response of the TBs depending on the relative direction between external stress and the nanotwin bundles. Current study emphasizes the close relationship between diamond microstructures and properties. With carefully selected precursors, the diamond microstructure can be modified, which in turn can further tune the mechanical properties of diamond.

Materials and Methods

Sample Preparation. Continuous films were drawn out from superaligned MWCNT arrays and folded into disks (2 mm in diameter) as precursor (24, 29, 30). Energy-dispersive spectroscopy measurement revealed dominant carbon and trace oxygen, indicating the high purity of the precursor. MWCNT disks were piled up with identical orientations into a bulk ($\phi 2 \text{ mm} \times 2 \text{ mm}$) and loaded into a cylindrical BN crucible. To determine the relationship between the orientation of MWCNT films and the microstructures of the synthetic diamond (i.e., the preferential orientation of nanotwin bundles) and consequentially to investigate the mechanical anisotropy with respect to the twin orientation, the initial positioning of MWCNT pileup in the BN crucible was labeled before the HPHT experiments, which were performed using a 10-MN double-stage large-volume multi-anvil system. Details about the experimental setup were described previously (5, 31). During the experiment, the pressure was increased to 15 GPa at room temperature with a rate of 0.75 GPa/h, then the temperature was ramped to $2,100^\circ\text{C}$ in 2.5 h and maintained at 15 GPa and $2,100^\circ\text{C}$ for 30 min. After that, the pressure was released with a rate of 0.7 GPa/h to the ambient pressure. The recovered sample (diamond rod) was ~ 1.5

mm in diameter and 1.5 mm in height. A total of 10 samples were prepared with the same condition. These samples show great repeatability in microstructure and mechanical properties.

Structure Characterization. The structure of the precursor and recovered compacts were characterized with an X-ray diffractometer (Bruker D8 ADVANCE, Cu K_{α}). Focused ion beam (FIB, FEI Scios) milling was employed to prepared TEM specimens, which were cut from the diamond rod along the direction parallel to the orientation of MWCNT films. During the FIB process, an accelerating voltage of 30 kV and a current of 30 nA was used initially to excavate two craters separated by a wall of ca. 2 μm in thickness. The wall was taken out and polished into a slice less than 100 nm in thickness with decreasing current from 15, 7, 5, and 1 to 0.5 nA. The surface of slice was cleaned with ion beam of 5 kV and 16 pA to minimize irradiation damage, followed by the low-energy Ar milling (Fischione Model 1040 NanoMill) to further minimize the knock-out damage on the slice. TEM characterization was carried out with an FEI Talos F200X (S)TEM instrument with an accelerating voltage of 200 kV. TEM specimens were also prepared to observe the cracks in the oriented, twinned diamond. The cracks were produced on the top surface and lateral cross section of the cylindrical sample and slices parallel to the nanotwin bundles on the top surface and perpendicular to the nanotwin bundles of the lateral cross section were prepared.

Mechanical Measurements. Before hardness measurements, mirror-like surfaces with a roughness less than 20 nm were carefully prepared from the synthetic samples with diamond grinding pastes. The polished samples are ~ 1 mm in thickness, three orders of magnitude higher than the indentation depth (ca. 600 to 800 nm for Knoop indenter and 1 μm for Vickers indenter), and the effect of sample thickness on hardness testing can be eliminated. Knoop hardness (H_K) was measured with a microhardness tester (KB 5 BVZ; KB Prüftechnik GmbH). The polished samples were placed on a flat steel carrier with a close fit, following the standard measurement procedure and avoiding the influence of the substrate. The loading and dwell time were 30 and 15 s, respectively. Five different angles (i.e., 0°, 30°, 45°, 60°, and 90°) between the major axis of indenter and orientation of MWCNT films (i.e., the preferential orientation of diamond nanotwin bundles) were taken for the Knoop hardness measurements. At least seven tests were performed for each angle with a load of 4.9 N. H_K was estimated from $H_K = 14228.9F/L^2$, where F (in Newton) is the applied load, and L (in μm) is the major diagonal length of Knoop indentation. To investigate the resistance to fracture, indentation fracture toughness measurements were carried out on the polished surfaces with a pyramid-shaped Vickers indenter. Loads of 4.9 and 9.8 N were applied with the two diagonals parallel and perpendicular to the orientation of MWCNT films,

respectively. The Vickers hardness, H_V , was determined from $H_V = 1854.4F/D^2$ with D (in μm) the average diagonal length of Vickers indentation; the indentation fracture toughness, K_{Ic} , was calculated as $K_{Ic} = 0.016(E/H_V)^{0.5}F/C^{1.5}$, where C (in μm) is the average length of the radial cracks measured from the indentation center, and E is the Young's modulus of diamond as 1,000 GPa.

MD Simulation of Hardness Test. The hardness test was simulated by MD with large-scale atomic/molecular massively parallel simulator code (32). Long-range carbon bond-order potential was chosen to describe the interatomic interactions (33), which has been successfully used to investigate the mechanical behavior of diamond (34, 35). An elongated rhombic-based diamond indenter was constructed with a length, width, and height of 24.47, 3.39, and 0.80 nm, respectively (SI Appendix, Fig. S6). In order to eliminate the size effect and the interaction of the indenter with its periodic images, a diamond cuboid with (a, b, c) of (29.70, 29.75, and 42.94 nm) was constructed with 665,856 carbon atoms. The TBs were set parallel to the c direction of the cuboid, and the minimum twin thickness of 0.618 nm was chosen for the simulation. During indentation test simulation, the load was applied perpendicular to the ab plane. Free boundary condition was set in the c direction and periodic boundary conditions were applied in the a and b directions. Before indentation, the diamond model specimen was equilibrated at 300 K. The indenter was initially positioned 0.2 nm above the center atom of the surface of the diamond. The indenter was moved at a rate of 0.02 nm/ps, and the microcanonical (a.k.a. NVE) ensemble was chosen during the indentation. The force acting on the indenter was then calculated as the summation of the force contributions from atoms belonging to the indenter, with the maximum displacement of 0.8 nm (the depth of the tip). The atomic configurations were visualized and analyzed with the open visualization tool package (36). The structural change in the indented diamond was identified with a previously reported method (37). Dislocation lines and Burgers vectors were identified with the dislocation extraction algorithm (38).

Data Availability. All study data are included in the article and/or SI Appendix.

ACKNOWLEDGMENTS. This work was supported by the National Natural Science Foundation of China (Grant Nos. 52090020, U20A20238, 51772260, 91963203, 51722209, and 51525205) and the National Key Research and Development Program of China (Grant Nos. 2018YFA0703400, 2018YFA0305900, and 2018YFA0208400). Z.Z. acknowledges National Natural Science Foundation of China for Distinguished Young Scholars of Hebei Province of China (E2018203349). K.T. acknowledges the National Postdoctoral Program for Innovative Talents (Grant No. BX20200285).

1. F. P. Bundy, H. T. Hall, H. M. Strong, R. H. Wentorfjun, Man-made diamonds. *Nature* **176**, 51–55 (1955).
2. T. Irifune, A. Kurio, S. Sakamoto, T. Inoue, H. Sumiya, Materials: Ultrahard polycrystalline diamond from graphite. *Nature* **421**, 599–600 (2003).
3. N. Dubrovinskaja *et al.*, Superhard nanocomposite of dense polymorphs of boron nitride: Noncarbon material has reached diamond hardness. *Appl. Phys. Lett.* **90**, 101912 (2007).
4. V. L. Solozhenko, O. O. Kurakevych, Y. Le Godec, Creation of nanostructures by extreme conditions: High-pressure synthesis of ultrahard nanocrystalline cubic boron nitride. *Adv. Mater.* **24**, 1540–1544 (2012).
5. Q. Huang *et al.*, Nanotwinned diamond with unprecedented hardness and stability. *Nature* **510**, 250–253 (2014).
6. Z. Zhao, B. Xu, Y. Tian, Recent advances in superhard materials. *Annu. Rev. Mater. Res.* **46**, 383–406 (2016).
7. G. Gerig, O. Kubler, R. Kikinis, F. A. Jolesz, Nonlinear anisotropic filtering of MRI data. *IEEE Trans. Med. Imaging* **11**, 221–232 (1992).
8. J. S. Lee, J. W. Park, S. M. Shin, Fabrication of a micro catalytic gas sensor using thin film process and Si anisotropic etching techniques. *Sens. Actuators B Chem.* **45**, 265–269 (1997).
9. K. Sano, Y. Ishida, T. Aida, Synthesis of anisotropic hydrogels and their applications. *Angew. Chem. Int. Ed. Engl.* **57**, 2532–2543 (2018).
10. J. H. Westbrook, P. J. Jorgensen, Effects of water desorption on indentation microhardness anisotropy in minerals. *Am. Mineral.* **53**, 1899 (1968).
11. G. M. Carter, J. L. Henshall, R. J. Wakeman, Knoop hardness and fracture anisotropy of calcite. *J. Mater. Sci. Lett.* **12**, 407–410 (1993).
12. V. V. Brazhkin *et al.*, Elastic moduli and the mechanical properties of stishovite single crystals. *Phys. Uspekhi* **45**, 447 (2002).
13. C. A. Brookes, Plastic deformation and anisotropy in the hardness of diamond. *Nature* **228**, 660–661 (1970).
14. M. A. Zaidi, J. A. Wert, "Thermomechanical processing of aluminum alloys" in *Treatise on Materials Science & Technology*, A. K. Vasudevan, R. D. Doherty, Eds. (Elsevier, 1989), vol. 31, pp. 137–170.
15. F. Isobe, H. Ohfujii, H. Sumiya, T. Irifune, Nanolayered diamond sintered compact obtained by direct conversion from highly oriented graphite under high pressure and high temperature. *J. Nanomater.* **2013**, 15 (2013).
16. P. Németh *et al.*, Complex nanostructures in diamond. *Nat. Mater.* **19**, 1126–1131 (2020).
17. P. Németh *et al.*, Diamond-graphene composite nanostructures. *Nano Lett.* **20**, 3611–3619 (2020).
18. V. V. Brazhkin *et al.*, Elastic properties of carbon phases obtained from C_{60} under pressure: The first example of anisotropic disordered carbon solid. *J. Phys. Condens. Matter* **14**, 10911–10915 (2002).
19. L. Lu, X. Chen, X. Huang, K. Lu, Revealing the maximum strength in nanotwinned copper. *Science* **323**, 607–610 (2009).
20. P. V. Teredesai *et al.*, Pressure-induced reversible transformation in single-wall carbon nanotube bundles studied by Raman spectroscopy. *Chem. Phys. Lett.* **319**, 296–302 (2000).
21. M. Popov, M. Kyotani, R. J. Nemanich, Y. Koga, Superhard phase composed of single-wall carbon nanotubes. *Phys. Rev. B Condens. Matter Mater. Phys.* **65**, 321–325 (2002).
22. V. D. Blank *et al.*, Nanostructured superhard carbon phase obtained under high pressure with shear deformation from single-wall nanotubes hipco. *Physica B* **382**, 58–64 (2006).
23. R. S. Kumar *et al.*, X-ray Raman scattering studies on C_{60} fullerenes and multi-walled carbon nanotubes under pressure. *Diamond Related Materials* **16**, 1250–1253 (2007).
24. K. Jiang, Q. Li, S. Fan, Nanotechnology: Spinning continuous carbon nanotube yarns. *Nature* **419**, 801–801 (2002).
25. C. A. Brookes, E. J. Brookes, Diamond in perspective: A review of mechanical properties of natural diamond. *Diamond Related Materials* **1**, 13–17 (1993).
26. B. Xu, Y. Tian, Ultrahardness: Measurement and enhancement. *J. Phys. Chem. C* **119**, 5633–5638 (2015).
27. Y. Tian, B. Xu, Z. Zhao, Microscopic theory of hardness and design of novel superhard crystals. *Int. J. Refract. Met. Hard Mater.* **33**, 93–106 (2012).
28. Y. Yue *et al.*, Hierarchically structured diamond composite with exceptional toughness. *Nature* **582**, 370–374 (2020).
29. X. Zhang *et al.*, Spinning and processing continuous yarns from 4-inch wafer scale super-aligned carbon nanotube arrays. *Adv. Mater.* **18**, 1505–1510 (2006).
30. K. Liu *et al.*, Periodically striped films produced from super-aligned carbon nanotube arrays. *Nanotechnology* **20**, 335705 (2009).

31. Y. Tian *et al.*, Ultrahard nanotwinned cubic boron nitride. *Nature* **493**, 385–388 (2013).
32. S. Plimpton, Fast parallel algorithms for short-range molecular dynamics. *J. Comput. Phys.* **117**, 1–19 (1995).
33. J. Los, A. Fasolino, Intrinsic long-range bond-order potential for carbon: Performance in Monte Carlo simulations of graphitization. *Phys. Rev. B Condens. Matter Mater. Phys.* **68**, 024107 (2003).
34. J. Xiao *et al.*, Intersectional nanotwinned diamond-the hardest polycrystalline diamond by design. *NPJ Comput. Mater.* **6**, 119 (2020).
35. J. Xiao *et al.*, Dislocation behaviors in nanotwinned diamond. *Sci. Adv.* **4**, eaat8195 (2018).
36. A. Stukowski, Visualization and analysis of atomistic simulation data with OVITO - The open visualization tool. *Model. Simul. Mat. Sc.* **18**, 015012 (2010).
37. E. Maras, O. Trushin, A. Stukowski, T. Ala-Nissila, H. Jonsson, Global transition path search for dislocation formation in Ge on Si(001). *Comput. Phys. Commun.* **205**, 13–21 (2016).
38. A. Stukowski, V. Bulatov, A. Arsenlis, Automated identification and indexing of dislocations in crystal interfaces. *Model. Simul. Mat. Sc.* **20**, 085007 (2012).